Dust Aerosol Retrieval Over the Oceans with the MODIS/VIIRS Dark Target algorithm. Part II: Non-Spherical Dust Model

Yaping Zhou[1,2], Robert C. Levy [2], Lorraine A. Remer[1],
Shana Mattoo[2,3], W. Reed Espinosa[2]
[1]University of Maryland Baltimore County, [2] NASA Goddard Flight Center, [3]Science Systems and Applications, Inc. Center,

Abstract

The Dark-target (DT) aerosol algorithm retrieves spectral Aerosol Optical Depth (AOD) and other aerosol properties from Moderate-resolution Imaging Spectrometer (MODIS) reflectance observations. Over the ocean, the DT algorithm is known to contain scattering-angle-dependent biases in its retrievals of AOD, Angstrom Exponent (AE) and Fine Mode Fraction (FMF) for dust aerosols. Following a two-step strategy to improve the DT retrieval of dust over ocean, for which the first step is to identify dusty pixels (reported in 'Part I'), in this 'Part II', we report on construction of a new dust model lookup table (LUT) and the strategy for applying it within the existing DT algorithm. In particular, we evaluate different characterizations of dust optical properties from a variety of frameworks and databases, and compare them with the current DT retrieval assumptions. Substituting the standard operational LUT with a spheroid dust model with identified dusty pixels shows significant improvement when compared with collocated AERONET-identified dusty pixels. Specifically, the application of the new dust model to dusty pixels reduces their AOD bias from 0.06 to 0.02 while improving the fraction of retrievals within expected error (EE) from 64% to 82%. At the same time, the overall bias in AE is reduced from 0.13 to 0.06, and the scattering-angle-dependent AE bias is largely eliminated. In testing on two full months of data (April and July), the new retrieval will reduce the monthly mean AOD by up to 0.1 and 0.2 in the north Atlantic and Arabian

seas, respectively. The average AE and FMF are also reduced in these dust heavy regions.

1. Introduction

Dust aerosols in the atmosphere can pose great impacts on weather, climate, air quality, public health, and ecosystems (Miller & Tegen, 1998; Harrison et al., 2001; Kaufman et al., 2002; Yu et al., 2006; Shell & Somerville 2007; Rosenfeld et al., 2011; Zhao et al., 2011; Griffin 2007; Goudie 2013; Shao et al., 2013; Kok et al., 2018). Dust retrieval with satellite remote sensing is very difficult because dust particles have a wide range of sizes, shapes and mineralogical compositions, depending on the source region and meteorological conditions. The size, shape and chemical compositions of particles determine their absorption and scattering properties and the radiances received by remote sensing instruments that retrieval algorithms rely upon.

The Moderate-resolution Imaging Spectrometer (MODIS) instruments on board NASA's EOS Terra and Aqua satellites have been observing the earth's cloud, aerosol and surface since their launches in 2000 and 2002, respectively. The Dark Target (DT) retrieval algorithm, which exclusively obtains aerosol properties over "dark targets", provides several official MODIS aerosol products. It actually consists of two independent algorithms, one for ocean (DT-O; Tanré et al.,1997; Remer et al., 2005; Levy et al., 2013), and one for dark land surfaces such as vegetation (DT-L; Levy et al., 2007a,b; Levy et al., 2010, Levy et al., 2013). The DT algorithm (both land and ocean) follows a lookup table (LUT) approach, i.e., the top-of-atmosphere (TOA) spectral reflectance is pre-calculated using scattering and radiative transfer (RT) codes (Wiscombe, 1980; Dubovik et al., 2002; Evans & Stephens, 1991; Ahmad and Fraser, 1982) for predefined aerosol, surface and atmospheric properties. Current ocean LUTs contain four fine aerosol models and five coarse aerosol models. The DT-O retrieval algorithm selects one fine mode and one coarse mode with an adjustable fraction from each mode to minimize the difference between the LUT reflectance and observed TOA reflectance in six wavelengths (0.55, 0.65, 0.86, 1.2, 1.6 and 2.11 μm). Dust aerosols are predominantly

non-spherical in shape (Chou et al., 2008). However, none of the current DT-O aerosol models are non-spherical, including those meant to represent dust optical properties.

Furthermore, simply adding a non-spherical model or replacing an existing coarse model will not solve the problem, as there is no guarantee that the algorithm will reliably choose non-spherical models for dust and spherical models for non-dust aerosol, possibly further degrading the results of the retrieval. Therefore, a two-step dust retrieval strategy is designed to first detect the dust and then apply a non-spherical dust model to identified dusty pixels. Part I of this series focused on dust detection. In this paper, we focus on constructing a non-spherical model and LUT for dust aerosol retrievals.

The paper is organized as follows: Section 2 describes the data used in this work. Section 3 describes construction of the dust optical models and LUT. Section 4 evaluates the performance of retrievals using the new dust models. Section 5 shows global aerosol retrieval in two dust heavy months. Section 6 summarizes the current work and plans for future improvement.

2. Data

The primary data used in the study are MODIS Level 1B calibrated TOA reflectance products (MxD02) (http://mcst.gsfc.nasa.gov/content/l1b-documents) and Collection C6 Level 2 aerosol products MxD04 (Levy et al., 2013) (where x is substituted by O for Terra and Y for Aqua). The MxD02 contains native resolution reflectance and radiance data (e.g. 0.25 km, 0.5 km or 1.0 km at nadir, depending on band), whereas the dark-target algorithm aggregates these observations into NxN boxes. The MxD04_L2 products used here include Aerosol Optical Depth (AOD), Angstrom Exponent (AE), and Fine Mode Fraction (FMF) reported at 10x10 km (nadir) resolution. In addition to the retrieved aerosol properties, a MxD04 data point contains the clear-sky reflectance values used in the retrieval, quality assurance (confidence) estimates, as well as other ancillary information such as 2-meter surface wind speed from National Centers for Environmental Prediction (NCEP) re-analysis.

The ‘clear-sky reflectance’ values in the MxDO4_L2 files provide the average reflectance for the NxN aggregation of native-resolution data, after it has been screened for clouds, surface inhomogeneities (glint patterns, underwater sediments, etc.), and outliers. In addition, the clear-sky reflectances have been adjusted to remove the effects of trace gas absorption. In other words, the resulting clear-sky reflectance (in each of the 6 wavelength bands) is the gas absorption corrected mean of the data that has not been masked or subject to statistical screening. The new dust retrieval uses the ‘clear-sky reflectance’ from MxD04 as input to the DT algorithm. From this point forward, when we say ‘retrieved pixel’, we mean the 10 x 10 km resolution aggregation reported in the MxD04 product or the new retrieval at the same spatial resolution.

Aerosol measurements from the ground-based Aerosol Robotic Network (AERONET) sun photometers are commonly used for validating satellite aerosol retrievals (Remer et al., 2005; Torres et al., 2013; Huang et al., 2016; Sayer et al., 2018; Gupta et al., 2018). AERONET is a global network of Cimel Electronique CE-318 sun-sky radiometers with between 4 and 9 spectral channels. In a common spectral configuration, AOD is obtained from direct sun measurements at 0.34, 0.38, 0.44, 0.50, 0.67, 0.87, and 1.02 μm with frequency of every 15 min; The high accuracy of AERONET AOD (estimated errors of ~0.01–0.02) makes it widely popular (Eck et al., 1999; Holben et al., 1998). In addition to direct sun measurement, the instruments measure the sky radiance in four spectral bands (0.44, 0.67, 0.87 and 1.02 μm) along the solar principal plane up to nine times a day and along the solar almucantar up to eight times a day. Measurements from almucantar scans are used to retrieve aerosol particle size distribution, spectral complex refractive index and single scattering albedo (SSA) (Dubovik & King, 2000; Dubovik et al., 2006). The majority of tradiational AERONET stations are situated inland, with some located on islands or near the coast, and very few in the middle of the ocean. To better test our ocean algorithm, we supplement these land-based observations with Sun photometer measurements made from aboard ship cruises as part of the AERONET Maritime Aerosol Network (MAN; Smirnov et al., 2009). In this

work, we use the latest Version 3 products, which provide improved cloud screening and better identification of heavy aerosol events (Giles et al., 2019).

To match the MODIS retrievals with the AERONET and MAN measurements, AERONET or MAN observations within ±30 min of the MODIS overpass time are averaged and compared against the values for all the MODIS retrieved pixels located within 0.3° of AERONET stations (Shi et al., 2019). In this way there are many collocations reported at each AERONET or MAN location at every overpass opportunity, since the AERONET or MAN observations are averaged to a single value but the many MODIS retrieved pixels within the match-up circle are not. The time period of the MODIS-AERONET collocation data spans from the beginning of the MODIS Terra and Aqua missions, which began in 2000 and 2002, respectively until 2014, while the MODIS-MAN collocation period covers the years from 2004 to 2014. AERONET AOD measurements at 0.44 μm and 0.67 μm are linearly interpolated in log-log space (i.e. fit by Angstrom exponent) so that they may be compared with MODIS AOD at 0.55 μm. Comparisons are only performed on pixels likely to be dominated by dust aerosol, which are identified by means of thresholds applied to the AERONET or MAN measurements (AOD > 0.3, AE < 0.6).

3. Constructing a dust aerosol model

Part I of this work reports on a novel dust detection algorithm. It combines spectral tests from near-UV (deep blue), visible, shortwave infrared (SWIR), and thermal infrared (TIR) wavelengths selected from a survey of existing dust detection algorithms. For each 10-km MxD04 retrieval pixel, there are 10x10 1-km pixels that the dust detection algorithm is applied to individually, using L1B reflectance and BT data from MxD02. The 10-km retrieval pixel is considered dusty if at least 3 1-km pixels are identified as dusty by the new dust detection algorithm. Quantitative evaluation of this new dust detection algorithm using collocated ground-based sun photometer (AERONET) as well as space based lidar (CALIOP on CALIPSO) finds it detects about

30% of dusty pixels in weak aerosol loading and more than 80% of heavy dust pixels, with very few false positive detections. The dust aerosol model derived in this paper is only applied to pixels that have been identified as dusty by this dust detection algorithm.

Once the dust dominated pixels are identified, the next step is to select a proper dust model and compute the corresponding LUT that can be used in the retrieval. In the current DT framework, the vector RT code of Ahmad and Fraser (1982, AF82) was used to create the LUTs. AF82 provides an internal Mie scattering code to compute spherical aerosol optical properties if particle size distribution and refractive indices are specified. However, alternative optical properties (scattering/extinction coefficients, phase matrices, etc.) can also be fed directly into AF82 in order to create new non-spherical LUTs. Our approach is to find a non-spherical aerosol model that is representative of most dust conditions in the real world. We compute the optical properties of the dust model outside of AF82 and then insert them into AF82 so that the rest of radiative transfer calculations are consistent with other DT aerosol models.

3.1 Dust optical properties

Dust in the atmosphere consists of a mixture of minerals with different sizes, shapes, densities, hygroscopicities, and chemical compositions (Sokolik and Toon, 1999). Optical properties (scattering and absorption) of dust are determined by these physical and chemical properties. In turn, the physical and chemical properties of the dust depend on the region of origin, how it was mobilized, and the transformation processes during dust transport. Since it is nearly impossible to prescribe a unique dust model for each dust sample or dust region, we seek a more generic dust model that represents the dust ensembles found in the real atmosphere.

The optical properties of an ensemble of particles can be integrated as:

$$Q = \int_{r_{min}}^{r_{max}} \int_{\varepsilon_1}^{\varepsilon_n} C(r, \varepsilon, r_e, r_i \ldots)\ \ wt(\varepsilon) \frac{dN(r)}{dr} d\varepsilon dr \qquad (1)$$

where C represents the relevant optical property (i.e., extinction, absorption coefficient or phase function) of the individual particles and is a function of refractive index (r_e, r_i), size (r) and shape (ε), wt (ε) is the weighting function (here it is assumed to only change with shape), and dN(r)/dr is the number size distribution (Dubovik et al., 2002) which we assume to take the form of a log-normal distribution:

$$\frac{dN(r)}{dr} = n(r) = \frac{1}{\sigma\sqrt{2\pi}} \frac{1}{r} \exp\left(-\frac{(\ln r - \mu)^2}{2\sigma^2}\right) \quad (2)$$

Here μ and σ are the mean and standard deviation of $\ln(n(r))$, respectively, which follows a normal distribution by definition. For a non-spherical particle, r can be taken as the equivalent radius of a spherical particle that has equal surface area or equal volume. It should be noted that, for a fixed population of particles, the value of u will change depending on whether it is represented in terms of volume or area equivalency (Wyser 1998).

Dust particles are often approximated by spheres (i.e., in the DT ocean algorithm, Remer et al., 2005; 2008; Levy et al., 2010; 2013) or spheroids (Dubovik et al., 2002 & 2006). Dubovik et al. (2006) derived an ensemble of 25 spheroid particle shapes with aspect ratios ranging from 0.3 to 3.0 to improve the AERONET retrieval. The same particle shape distribution is used in the GRASP (Generalized Retrieval of Aerosol and Surface Properties; Dubovik et al., 2014) model, which is developed from Dubovik et al. (2002; 2006), but is more flexible and capable of characterizing surface and atmospheric properties from a variety of remote sensing observations. In addition, recent advances in radiative transfer theory and computational methods have made possible the computation of optical properties of more complicated particle shapes (Bi et al., 2010; Liu et al., 2013; Tang et al., 2019). The Texas A&M single-scattering properties database consists of pre-computed optical properties of a wide range of tri-axial ellipsoidal particles with different refractive indices, sizes and shape parameters (Meng et al., 2010) that allows users to compute the optical characteristics of a specific aerosol ensembles of their choice. We have conducted many sensitivity studies to determine the size distribution, shape combination and optical database most suitable for our dust model.

An initial study has been conducted to examine the sensitivity of optical properties to particle shape for different aerosol sizes. We start by replacing each of the spherical particles in the fine (Model 1, Fig.1a) and coarse (Model 8, Fig.1b) mode models of the standard DT algorithm with a non-spherical particle of equivalent projected area. Furthermore, in this new aerosol model, each non-spherical particle maintains the same refractive index as its spherical counterpart (Table 1). Since the Texas A&M (TX) database provides a wide range of complex particle shapes, we chose to test three different shapes from the database: 1) spheres (TX-Sphere), 2) a mixture of spheroid shapes that are consistent with what has been used in the GRASP model (TX-Sphd), and 3) a mixture of ellipsoids (TX-Ellipd). As mentioned earlier, the current DT algorithm assumes all particles to be spherical and excellent agreement was found between the single scattering properties of the DT and TX-sphere cases (Figure not shown).

For the fine mode, Figure 2 shows that particle shape does not have a large impact on the optical properties at the seven MODIS wavelengths (0.47μm, 0.55 μm, 0.65 μm, 0.86 μm, 1.24 μm, 1.63 μm and 2.11 μm) used in the DT aerosol retrievals. The extinction cross sections (CEXT) from the TX-Sphere (not shown) and original DT are almost identical and only slightly smaller than the values corresponding to the spheroid (TX-Sphd) and ellipsoid (TX-Ellipd) particle shapes (Fig. 2a). Furthermore, the spectral shapes of CEXT are almost indistinguishable among the three particle morphologies (Fig. 2b). The phase functions (P_{11}) are also very similar, with TX-Ellipsd showing slightly more backscattering than the TX-Sphere and TX-Sphd shapes (Fig. 2c). The only relatively large difference appears in the degree of linear polarization ($-P_{12}/P_{11}$) near its peak at scattering angles around 90° (Fig. 2d). Since the MODIS instruments do not explicitly measure the polarization state of the observed scene and P_{12}/P_{11} has only a small impact on the total reflectance LUT, it is not necessary to add new non-spherical dust particles to the existing fine mode aerosol model.

However, for the coarse mode, CEXT, phase function and the degree of linear polarization all have significant sensitivity to particle shape (Fig. 3). A large difference can be observed between the TX-sphere and non-spherical particle phase functions for

scattering angles greater than 80° (Fig. 3c). The particles with non-spherical shapes have much flatter phase functions in these scattering angle ranges than the spherical particles, resulting in larger phase function values between 80 ~ 140° and smaller phase function values at scattering angles greater than 140°. These phase function differences between spherical and non-spherical particles are the main cause of scattering-angle-dependent-bias in DT retrievals of dust aerosol (shown later). We also notice large differences in the linear polarization state of the scattered light, with the spherical and non-spherical particle classes having opposite signs at most scattering angles (Fig. 3d). Lastly, we see large differences in CEXT, both in magnitude and spectral dependence, among the different shapes (Fig. 3a). The TX-Ellipsoid has the largest CEXT and DT-Sphere has the smallest CEXT. Due to the way the DT algorithm is designed, the spectral dependence of CEXT rather than the absolute value of CEXT at 0.55 μm matters in the retrieval of AOD at 0.55 μm, and at the other wavelengths (Eq. 5-7). The weaker the spectral dependence of CEXT, the weaker will be the spectral dependence of the retrieved AOD and the smaller the magnitude of the retrieved AE. The DT algorithm is particularly sensitive to the spectral dependence of the observations and the LUT values that will be matched to the observations.

Between 0.47 μm and 0.86 μm, we notice a "spectral dip" appearing near 0.65 μm for the spheroid and ellipsoid shapes from the TX database. We believe that this dip is unphysical, given the small change in refractive indices among these channels (Table 1). Further investigation of the TX database revealed that the dips are caused by significant computational noise in some of the database entries, specifically those representing prolate particles with aspect ratios larger than 2.2 (personal communications with Jiacheng Ding, 5/1/2019). Unfortunately, these artifacts prohibit the use of the TX database for our application because realistic modeling of the spectral dependence is central to the performance of the DT algorithm.

For this reason, we ultimately derive our new optical properties from the database of single scattering properties furnished with the GRASP toolset. The green curve in

Figure 3 (GRASP-Sphd) represents the same particle microphysics as TX-Sphd but with the optical properties pulled from the GRASP database. The phase function from GRASP is very similar to those from TX-Sphd and TX-Ellipd, but the GRASP derived values of CEXT fall between the spherical and non-spherical particles in the TX database. Most importantly, GRASP does not have the undesired spectral dip. The spectral variation of CEXT from GRASP-Sphd is also smaller than that from DT (Fig. 3d), which will impact the retrieved AE as will be shown later.

Besides the shape of the particles, the spectral refractive indices and size distribution are very important in determining the optical properties of dust. There are many laboratory and field measurements of dust optical properties (Dubovik et al., 2002; Hess et al., 1998; Levoni et al., 1997; Muñoz et al., 2007; Petzold et al., 2009; Formenti et al., 2011; Espinosa et al., 2018). Many of these measurements are not directly applicable to our needs because specific locations or samples are not representative of global dust properties, or instrument geometry, wavelength and calibration differ from the MODIS instrument. For example, refractive indices derived from AERONET stations have to be adjusted when applied to DB algorithm for the Visible Infrared Imaging Radiometer Suite (VIIRS) instrument due to calibration issues (Lee et al., 2017). We tried several dust models from the literature (see above), including the dust models used by Lee et al., (2017), two "dust-like" coarse mode models from the current DT algorithm (replacing the spherical shaped particles with a mixture of spheroids and ellipsoids) and perturbations of different refractive indices and size distributions based on these models. The tests are somewhat "ad hoc" as only retrieval results can indicate whether the chosen dust model is "good enough" by comparison with AERONET retrievals. Ultimately, the model chosen was similar to the 'dust-like' Model-8 of the operational DT algorithm but with a slightly reduced median radius. The new model is named Model-10 in the following description and in Table 1.

3.2 Dust LUT

The look up table (LUT) calculates the relationship between aerosol optical depth at 0.55 μm ($\tau_{0.55}$) and TOA reflectance at a given wavelength and geometry

$$R = f(\tau, \lambda, \theta_0, \theta, \phi, \text{wind}). \quad (4)$$

The value $\tau_{0.55}$ is used as the anchor of the LUT and the RT code seeks the right concentration of particles to satisfy this optical loading. After the ensemble dust absorption and single scattering optical properties are computed, they are used in the AF82 radiative transfer model along with wind dependent surface reflectance and the Rayleigh scattering contribution of the atmosphere (dependent on wavelength) to simulate the TOA reflectances of the LUT.

We take CEXT_λ, SSA_λ, and $\text{P11}_{(\lambda,\Theta)}$ to represent the extinction coefficient, single scattering albedo, and phase functions, respectively, at wavelength λ and scattering angle Θ. For example, $\text{CEXT}_{0.55}$ is the extinction coefficient at 0.55 μm. If N is the total number of scattering particles per cross-sectional area of atmospheric column the following equation holds,

$$N \propto \tau_{0.55} / \text{CEXT}_{0.55} \quad (5)$$

In the single scattering limit, the Rayleigh corrected reflectance at the sensor over a dark surface can therefore be *approximated* by $R'_{(\lambda,\Theta)}$ where,

$$R'_{(\lambda,\Theta)} \propto \text{P11}_{(\lambda,\Theta)} \times \text{SSA}_\lambda \times \text{CEXT}_\lambda \times N$$

$$\propto \text{P11}_{(\lambda,\Theta)} \times \text{SSA}_\lambda \times \tau_{0.55} \times \frac{\text{CEXT}_\lambda}{\text{CEXT}_{0.55}}. \quad (6)$$

At 0.55 μm, we have

$$R'_{(0.55,\Theta)} \propto \text{P11}_{(0.55,\Theta)} \times \text{SSA}_{0.55} \times \tau_{0.55}. \quad (7)$$

From equation (7) it can be seen that, given a fixed reflectance $R_{(0.55,\Theta)}$, the retrieved optical depth is very strongly dependent on our choice of $P11_{(0.55,\Theta)}$ and $SSA_{0.55}$. Over estimation of τ could be due to an unrealistically small value of a P_{11} at the observed scattering angle (P_{11} is primarily dependent on the real refractive index, particle size and shape) or too much absorption (depends primarily on the imaginary refractive index). It is clear that the P_{11} values corresponding to spherical particles used in the current DT algorithm are too high at scattering angles $>140^{o}$ and too low at $80\text{-}140^{o}$ for dust particles, which will likely make the retrieved AOD too low at scattering angle $> 140^{o}$ and too high at $80\text{-}140^{o}$. The optical depth at wavelengths other than 0.55 μm depends on the ratio of extinction coefficient at that wavelength relative to extinction at 0.55 μm as we mentioned earlier. The flatter spectral variation of non-spherical particles (Fig. 3d) will reduce the spectral steepness of optical depth and reduce the AE.

Figure 4 shows the angular distribution of reflectance, i.e., bidirectional reflectance function (BRF), of spherical particles and the difference produced by changing the particle shapes from spheres to the mixed spheroid shapes of Model-10 at a given optical depth and wavelength. The negative (positive) BRF difference means a higher (lower) optical depth would be required to match the measured reflectances at the different sun-view geometries. We notice that more angular regions present negative difference than positive difference at 0.87 μm. Figure 5 shows the reflectance differences as a function of scattering angle at six wavelengths. Focusing on the range of scattering angles normally viewed by the MODIS sensor (greater than 80°), we notice that the reflectance differences are negative in all channels for scattering angle greater than 140°. This is expected from Figure 3c, as the phase functions of non-spherical particles at these angles are lower than those of the spherical particles, therefore, we could expect that the retrieved AOD (at 0.55 μm) at these angles to be higher under the spheroidal particle assumption. For scattering angles ranging from 80° to 140°, reflectance differences tend to be positive at shorter wavelengths (0.87 μm and shorter) while negative at the longer wavelengths. Since the reflectance at short wavelengths tends to be larger than at the NIR channels, their overall impact on the retrieved AOD is larger and the retrieved AOD (at

0.55 μm) is more likely to be smaller with the spheroid particles. Meanwhile, we could also expect the retrieved spectral AOD to be higher at longer wavelengths and smaller at shorter wavelengths in these scattering angles, resulting in a reduction of AE.

4. Dust retrieval with standalone DT-O algorithm

Before operational implementation, we applied the new dust model (Model-10) to the standalone DT-ocean algorithm, which takes cloud-screened and grid averaged clear sky reflectance, surface wind and geometric angles from MxD04 output (e.g. Levy et al., 2007). The standalone algorithm uses the same "guts" as the standard algorithm (spectral observations compared with LUTs iteratively to find the best-fit), however it only does one retrieval per call (Levy & Pinker 2007). This has a fast turnaround because it does not have to do the time-consuming preprocessing (reading L1B data, gas absorption corrections, performing pixel screening, cloud masking, etc.) and computes only the specified pixels. However, there is a small difference in the retrieved AOD between the operational algorithm and the standalone algorithm due to numerical truncation of the reflectance values in the MxD04 output (Falguni Patadia personal communication, 9/1/2018). The standalone model can be easily modified to only allow the new dust Model-10 as its "chosen" coarse model while the choice of fine model remains as usual for specified dusty pixels. We conducted extensive validation of the new dust model with many dusty granules and collocated AERONET dusty pixels.

4.1 Evaluation with dusty granules

We applied our new dust detection algorithm from Part I to hundreds of MODIS granules. When dust pixels are detected, we run the retrieval of that pixel with the modified standalone algorithm that forces the new dust model to be picked. The standalone model retrieves AOD, FMF, AE, and reports retrieval error ERR as in the operational retrieval.

Figure 6 shows one such granule. It illustrates retrieved AOD, FMF and AE1 from the DT (spherical, 6d, 6g, 6j), dust-detected (non-spherical, 6e, 6h, 6k), and the joint (6f, 6i, 6l) aerosol retrievals for the MODIS-Aqua granule from 13 July 2005 over the Arabian Peninsula (6c). The joint retrievals assume original DT retrievals for non-dust pixels while replacing the values with standalone model retrievals for identified dusty pixels. Areas of high AOD and low AE, as determined by the C6 DT-retrieval, are shown in 6a, with areas detected as dust, by the detection algorithm (of Part I) described in Section 3, are shown in 6b. Only pixels detected as dust are retrieved using the non-spherical LUT. Included in each panel are contours of scattering angle (Θ). For this granule, Figure 6f shows that the AOD is significantly reduced by applying the non-spherical model in the Red Sea (smaller Θ), with little or no reduction in the Persian Gulf (larger Θ). FMF and AE are reduced for most dust-detected pixels. Compared with the C6 retrievals, the AOD, AE and FMF from the non-spherical retrievals show less abrupt changes spatially of the dust plumes over the ocean. But some rough transitions between the non-spherical and spherical retrievals in FMF and AE1, especially in the Persian Gulf are still visible. It appears that while there might be "dust" everywhere in the region, the magnitude may not be large enough to trigger the dust detection in some areas, hence the rough transition between non-spherical and spherical.

4.2 Evaluation with collocated AERONET and MAN observations

To conduct a more quantitative evaluation, we used dust observations from Version 3 AERONET and MAN observation. As mentioned in Section 2, we selected a subset of dusty pixels from MODIS-AERONET and MODIS-MAN collocation datasets based on AERONET/MAN measurements (AOD > 0.3, AE < 0.6). The total number of AERONET/MAN identified dusty pixels from each collocation set can be found in Table 2, while the spatial distribution of available dusty pixels (including both AERONET and MAN observations) in each 10°x10° box is shown in Figure 7. The number of available dusty pixels in each grid box depends on both the number of AERONET/MAN stations and dust frequency in the region as we can see that most validation dusty pixels are concentrated in the tropical north Atlantic, Mediterranean, Persian Gulf and off the coast

of east Asia. For selected MODIS pixels, we apply the retrieval with the modified standalone DT-O algorithm using the new dust LUT.

Figure 8 shows the AOD and AE retrievals with the new dust model as compared with the AERONET measurements for dusty pixels selected from the AQUA-AERONET collocation dataset. The C6 retrievals are also displayed for comparison. The new retrieval has significantly reduced the high bias in AOD at 0.55 μm from C6 (0.08) to 0.02, percentage of retrievals above EE (± (0.05+15%)) from 32.5% to 13.7% and RMS from 0.23 to 0.17. The percentage within EE has increased from 64.3% to 82.3%. The high bias and RMS in AE from C6 are reduced from 0.13 to 0.06, and 0.27 to 0.19, respectively. It has been a long-standing problem of the DT algorithm that AEs are overly flat (biased high in low AE and low in high AE) (Schutgens et al., 2013). Here we improved AE in the low end for the coarse mode aerosol. In addition, the scattering-angle-dependent AE bias in C6 (Fig. 8c) is also largely eliminated in the new retrieval (Fig. 8f). There are similar improvements from the other collocated datasets, i.e., Terra-AERONET, Terra-MAN and Aqua-MAN. The detailed statistics are listed in Table 3. In all the cases, the new algorithm reduces bias and rms of the AOD and AE significantly. The percentages of AOD retrievals within the EE has risen from 64%-71% to 82%-89% with the exception of Aqua-MAN collocated dataset, in that case the EE raised from 86% to 95%. The new retrieval has a mean bias less than 0.02 in AOD and less than 0.07 in AE in all the cases.

To examine whether the new retrievals perform uniformly across the regions, we computed mean dusty pixel AOD and AE for each 10° latitude x10° longitude degree box from observations (combined collocated measurements from AERONET and MAN), C6 and the new non-spherical retrievals for Aqua (Fig.9) and Terra (Fig.10). The purpose of this test is to identify regions with consistently poor performance that may need a specific regional dust model. The results indicate that AOD has been improved across the board (more white circles and very few colored circles), with the exception of one location in the central Asia (over Lake Balkhash, Kazakhstan) where both C6 and the new retrievals are consistently higher than the ground observations. For AE, there are overall

improvements in matching AERONET/MAN by using the new Model-10 versus the C6 retrieval, but there remain a few spots with persistent large deviations from the ground truth. The discrepancies in AE in these regions, despite the improvement of AOD in these same regions, speak to the sensitivity of AE to subtle changes in retrieved spectral AOD, versus the relatively insensitivity of AOD retrieval at a single wavelength.

Note that here we chose to include AERONET/MAN measurements with smaller aerosol loading to test the non-spherical dust model. The results found in this section are similar if we restrict our dust samples to general dust criteria used in Part I (AOD > 0.5, AE < 0.6).

5. Impact on global dust estimates

To estimate the global impact of the new dust retrieval on AOD, AE and FMF, we applied the new dust retrieval globally to two dust heavy month-long periods: April 12 to May 11, 2011 (Figure 11) and July 1 to July 31, 2011 (Figure 12). The two periods are selected to capture the prevalence of dust in northwest Asia in April (spread over Northwest Pacific, Yu et al., 2012) and the heaviest period of African dust occurring in July (Huang et al., 2010). Dust pixels were first detected with our new dust detection algorithm (shown in Fig. 9 and Fig. 10 in Part I). The new dust model (Model-10) is applied to detected dusty pixels with the standalone algorithm and the retrievals from these dusty pixels are merged with the standard C6 the retrievals. In Figure 11, the left column shows the period averaged retrievals of AOD at 0.55 μm, AE1 and FMF from C6 retrievals. The right column shows the difference between C6 retrievals and retrievals using new dust model after dust detection (New – C6). We notice that major impacts occur in the oceans near the major dust sources: Tropical North Atlantic, the Mediterranean and Arabian seas, and the northeast China sea. There is an overall reduction in AOD in the aforementioned regions of about 0.02, and also generally reduced values of AE and FMF. In July 2011, the dust events in northeast Asia subsided to some degree but dust events in West Africa and the Arabian Peninsula increased significantly leading to increased dust occurrences over the North Atlantic Ocean, Persian

Gulf and Arabian Sea (Figure 12). The result is a much decreased monthly averaged AOD (up to 0.2), AE and FMF in these regions using the new dust model.

The top of atmosphere (TOA) shortwave radiative efficiency in the northern Atlantic region is estimated to be -49.7 W m^{-2} AOD^{-1} and -36.5W m^{-2} AOD^{-1} based on CERES radiation data and AOD from MODIS and CALIOP, respectively (Song et al., 2018). The monthly AOD reduction in these regions could be as much as 0.05 ~ 0.2 based on the new retrieval, which means previous estimates of the monthly shortwave radiative forcing in this region could be biased high by about 2 ~ 8 Wm^{-1}. The full scale impact of the new dust retrieval on global and regional AOD and its direct radiative effect will be investigated after the new scheme is implemented operationally and the entire MODIS data record reprocessed.

6. Summary and discussion

The Dark-target (DT) aerosol retrieval is an operational algorithm of the MODIS instruments on the Terra and Aqua satellites that has retrieved spectral aerosol optical depth (AOD) over land and ocean since 2000 and 2002, respectively. Recently, DT has been ported to the VIIRS instrument aboard Suomi-NPP (Sawyer et al., 2019), the Advanced Baseline Imager (ABI) on GOES-East and GOES-West, the Advanced Himawari Imager (AHI) on Himawari (Gupta et al., 2019). The continued application of the DT algorithm to observations made by the VIIRS instrument, both on the current Suomi-NPP platform and on future NOAA series satellites, will ensure a seamless long-term aerosol climate record. Moreover, the algorithm's application to geosynchronous satellites will enable better monitoring of major aerosol events, such as fires, dust storms and pollution.

Over the ocean, the DT algorithm is known to produce biased retrievals of AOD, AE and FMF in pixels containing significant dust aerosol because the current version of DT-O does not have an aerosol model capable of faithfully representing these non-spherical dust particles. In this work, we designed and evaluated a two-step dust aerosol

retrieval strategy in which we first detect dust pixels and then utilize a new non-spherical dust model in the retrieval of the detected dusty pixels. The dust detection methodology is reported in Part I, while this paper describes the construction of the non-spherical dust model and lookup table (LUT). Sensitivity tests are conducted to determine a dust size and shape distribution and set of refractive indices that best represent the spectral and angular single-scattering characteristics most relevant to a MODIS-like sensor. In particular, we examined ensemble dust optical properties from the Texas A&M scattering databases for a variety of shapes (sphere, spheroid and ellipsoid) and size distributions. A final dust model (Model-10) is created that resembles the current Model-8 coarse mode in the DT algorithm but with slightly smaller size and a mixture of spheroidal particles. The optical properties of the new dust model are ultimately computed using the GRASP toolset.

Both the new dust detection and dust models have been tested extensively with manually selected dusty granules. Aerosol measurements from AERONET and MAN are used for quantitative evaluation of the new dust retrievals. Results indicate the new algorithm reduces bias and rms in the retrieved AOD and AE significantly. The percentages of AOD retrievals within the EE rose from 64%-71% to 82%-88% with the exception of the Aqua-MAN collocated dataset, where the EE increased from 86% to 95%. In all the cases, the new retrieval has lowered the mean bias to less than 0.02 in AOD and less than 0.07 in AE in all the cases. Even more encouragingly, the new retrievals have eliminated all scattering-angle-dependent biases in dusty pixels through the incorporation of phase functions corresponding to non-spherical particles. We estimate that implementation of the new dust retrieval method in the operational algorithm will result in a reduction of monthly mean AOD, AE and FMF in dust heavy regions such as the northeast Pacific, North Atlantic, Persian Gulf and Arabian Sea. The magnitude of the resulting reductions in AOD can be as large as 0.05 to 0.2, corresponding to a decrease in TOA shortwave radiative forcing of up to 2~8 Wm^{-2}.

We should point out that neither the dust detection nor the dust aerosol model developed in this work is comprehensive due to the extreme spatial and temporal

variability in dust's physical sizes and chemical compositions. The need to rely on manual tuning of detection thresholds hinders the accuracy of the new dust detection algorithm. We expect that machine learning may be able to determine better thresholds and decision trees (Cho et al., 2013; Wang et al., 2019). As for the dust model, using one set of microphysical properties to represent the wide variety of dusts found globally is a significant limitation and the development of regionally applicable dust models may yield significant improvements.

Acknowledgement: This work is supported by NASA NNH13ZDA001NTERAQEA, DSCOVR Earth Science Algorithms managed by Richard Eckman. We would like to thank Professor Ping Yang for providing the Texas A&M scattering database, Peter Colarco at GSFC for a code to read and integrate the database and Jiacheng Ding from Texas A&M for many discussions regarding the database. The AERONET/MAN - MODIS collocation data is provided by Yingxi Shi at GSFC. W. Reed Espinosa's participation in this research was partially supported by an appointment to the NASA Postdoctoral Program at the NASA Goddard Space Flight Center, administered by Universities Space Research Association through a contract with NASA.

References

Ahmad, Z., & Fraser, R. S. (1982) An Iterative Radiative Transfer Code For Ocean-Atmosphere Systems, J. Atmos. Sci., 39, 656–665, https://doi.org/10.1175/1520-0469(1982)039<0656:AIRTCF>2.0.CO;2.

Bi, L., Yang, P., Kattawar, G., & R. Kahn, R. (2010). Modeling optical properties of mineral aerosol particles by using nonsymmetric hexahedra. Appl. Opt. 49, 334-342.

Cho, H.-M., Nasiri, S. L., Yang, P., Laszlo, I., & Zhao, X. (2013). Detection of optically thin mineral dust aerosol layers over the ocean using MODIS, J. Atmos. Oceanic Technol., 30, 896–916.

Chou, C., Formenti. P., Maille, M., Ausset, P., Helas, G., Harrison, M., & Osborne, S. (2008). Size distribution, shape, and composition of mineral dust aerosols collected during the African Monsoon Multidisciplinary Analysis Special Observation Period 0: Dust and Biomass-Burning Experiment field campaign in Niger, January 2006. J. Geophys. Res. Atmos., 113 (D23).

Dubovik, O., & King, M.D. (2000). A flexible inversion algorithm for retrieval of aerosol optical properties from Sun and sky radiance measurements," J. Geophys. Res., 105, 20 673-20 696.

Dubovik, O., Holben, B., Eck, T.F., Smirnov, A., Kaufman, Y.J., King, M.D., Tanré, D., & Slutsker, I. (2002). Variability of absorption and optical properties of key aerosol types observed in worldwide locations. Journal of the atmospheric sciences, 59(3), pp.590-608.

Dubovik, O., Sinyuk, A., Lapyonok, T., Holben, B. N., Mishchenko, M., Yang, P., Eck, T. F., Volten, H., Munoz, O., Veihelmann, B., Zande, W. J. v. d., Leon, J.-F., Sorokin, M., & Slutsker, I. (2006). Application of spheroid models to account for aerosol particle nonsphericity in remote sensing of desert dust, J. Geophys. Res., 111, D11208, doi: 11210.11029/12005JD006619.

Dubovik, O., Herman, M., Holdak, Lapyonok, T., Tanré, D., Deuzé, J. L., Ducos, F. Sinyuk, A., and Lopatin, A. (2011), Statistically optimized inversion algorithm for en- hanced retrieval of aerosol properties from spectral multi-angle polarimetric satel-

lite observations, Atmospheric Measurement Techniques, 4(5), 975–1018, doi:10.5194/ amt-4-975-2011.

Dubovik, O., Lapyonok, T., Litvinov, P., Herman, M., Fuertes, D., Ducos, F., Torres, B., Derimian, Y., Huang, X., Lopatin, A., Chaikovsky, A., Aspetsberger, M., & Federspiel, C. (2014), GRASP: a versatile algorithm for characterizing the atmosphere, SPIE News- room, pp. 2–5, doi:10.1117/2.1201408.005558.

Eck, T. F., Holben, B. N., Reid, J. S., Dubovik, O., Smirnov, A., O'Neill, N. T., Slutsker, I., & Kinne, S. (1999). Wavelength dependence of the optical depth of biomass burning, urban, and desert dust aerosols, J. Geophys. Res.-Atmos., 104, 31333–31349, https://doi.org/10.1029/1999JD900923.

Espinosa, W.R., Martins, J.V., Remer, L.A., Puthukkudy, A., Orozco, D., & Dolgos, G., (2018). In situ measurements of angular-dependent light scattering by aerosols over the contiguous United States. Atmospheric Chemistry and Physics, 18(5), pp.3737-3754.

Evans, K. F., & Stephens, G. L. (1991). A new polarized atmospheric radiative transfer model, J. Quant. Spectrosc. Ra., 46, 413–423.

Formenti, P., Schütz, L., Balkanski, Y., Desboeufs, K., Ebert, M., Kandler, K., Petzold, A., Scheuvens, D., Weinbruch, S., & Zhang, D. (2011). Recent progress in understanding physical and chemical properties of African and Asian mineral dust, Atmos. Chem. Phys., 11, 8231–8256, https://doi.org/10.5194/acp-11-8231-2011.

Giles, D. M., Sinyuk, A., Sorokin, M. G., Schafer, J. S., Smirnov, A., Slutsker, I., Eck, T. F., Holben, B. N., Lewis, J. R., Campbell, J. R., Welton, E. J., Korkin, S. V., & Lyapustin, A. I.(2019). Advancements in the Aerosol Robotic Network (AERONET) Version 3 database – automated near-real-time quality control algorithm with improved cloud screening for Sun photometer aerosol optical depth (AOD) measurements, Atmos. Meas. Tech., 12, 169–209, https://doi.org/10.5194/amt-12-169-2019.

Goudie, A.S., Deseart dust and human health disorders. Envion. Int., 63, 101-103, doi:10.1016/j.envint.2013.10.011.

Griffin, D. W. (2007). Atmospheric Movement of Microorganisms in Clouds of Desert Dust and Implications for Human Health, Clinical Microbiology Reviews. 20 (3): 459–77, doi:10.1128/CMR.00039-06.

Gupta, P., Remer, L. A., Levy, R. C., & Mattoo, S. (2018). Validation of MODIS 3 km land aerosol optical depth from NASA's EOS Terra and Aqua missions, Atmos. Meas. Tech., 11, 3145–3159, https://doi.org/10.5194/amt-11-3145-2018.

Gupta, P., Levy, R. C., Mattoo, S., Remer, L. A., Holz, R. E., & Heidinger, A. K. (2019). Applying the Dark Target aerosol algorithm with Advanced Himawari Imager observations during the KORUS-AQ field campaign, Atmos. Meas. Tech., 12, 6557–6577, https://doi.org/10.5194/amt-12-6557-2019.

Harrison, S.P., Kohfeld, K.E., Roelandt, C. and Claquin, T. (2001). The role of dust in climate changes today, at the last glacial maximum and in the future. Earth-Science Reviews, 54(1), pp.43-80.

Hess, M., Koepke, P., & Schult, I. (1998) Optical properties of aerosols and clouds: The software package OPAC, B. Am. Meteorol. Soc., 79, 831–844, https://doi.org/10.1175/1520-0477(1998)079<0831:Opoaac>2.0.Co;2.

Holben, B. N. (1998). AERONET—A federated instrument network and data archive for aerosol characterization, Remote Sens. Environ., 66, 1–16.

Huang, J., Zhang, C., & Prospero, J. M. (2010). African dust outbreaks: A satellite perspective of temporal and spatial variability over the tropical Atlantic Ocean, J. Geophys. Res., 115, D05202, doi:10.1029/2009JD012516.

Huang, J., Kondragunta, S., Laszlo, I., Liu, H., Remer, L. A., Zhang, H., Superczynski, S., Ciren, P., Holben, B. N., & Petrenko, M. (2016). Validation and expected error estimation of Suomi-NPP VIIRS aerosol optical thickness and Ångström exponent with AERONET, J. Geophys. Res. Atmos., 121, 7139– 7160, doi:10.1002/2016JD024834.

Kaufman, Y. J., Tanre, D., & Boucher, O. (2002). A satellite view of aerosols in the climate system, Nature, 419, 215–223.

Kok, J. F., Ward, D.S., Mahowald, N.M., & Evan, A.T. (2018). Global and regional importance of the direct dust-climate feedback, *Nature Communications*, 9, 241.

Lee, J., Hsu, N. C., Sayer, A. M., Bettenhausen, C., &Yang, P. (2017). AERONET-Based Nonspherical Dust Optical Models and Effects on the VIIRS Deep Blue/SOAR Over Water Aerosol Product. Journal of Geophysical Research: Atmospheres, 122 (19):10,384-10,401 [10.1002/2017jd027258]

Levoni, C., Cervino, M., Guzzi, R., & Torricella, F. (1997). Atmospheric aerosol optical properties: a database of radiative characteristics for different components and classes, Appl. Opt., 36, 8031–8041, https://doi.org/10.1364/Ao.36.008031.

Levy, R. C., & Pinker, R. T. (2007). Remote Sensing of Spectral Aerosol Properties: A Classroom Experience." *Bulletin of the American Meteorological Society*, 88 (1): 25-30 [10.1175/bams-88-1-25]

Levy, R.C., Remer, L.A., & Dubovik, O. (2007a). Global aerosol optical properties and application to Moderate Resolution Imaging Spectroradiometer aerosol retrieval over land. Journal of Geophysical Research: Atmospheres, 112(D13).

Levy, R.C., Remer, L.A., Mattoo, S., Vermote, E.F., & Kaufman, Y.J., (2007b). Second-generation operational algorithm: Retrieval of aerosol properties over land from inversion of Moderate Resolution Imaging Spectroradiometer spectral reflectance. Journal of Geophysical Research: Atmospheres, 112(D13).

Levy, R. C., Remer, L. A., Kleidman, R. G., et al., (2010). Global evaluation of the Collection 5 MODIS dark-target aerosol products over land. Atmos. Chem. Phys., 10 (21): 10399-10420 [10.5194/acp-10-10399-2010]

Levy, R.C., Mattoo, S., Munchak, L.A., Remer, L.A., Sayer, A.M., Patadia, F., & Hsu, N.C. (2013). The collection 6 modis aerosol products over land and ocean. Atmos. Meas. Tech., 6, 2989–3034.

Liu, C., Panetta, R. L., Yang, P., Macke, A., & Baran, A. J. (2013). Modeling the scattering properties of mineral aerosols using concave fractal polyhedral. Appl. Opt. 52, 640-652 (2013)

Meng, Z., Yang, P., Kattawar, G., Bi, L, Liou, K,N, Laszlo, I. (2010). Single-scattering properties of tri-axial ellipsoidal mineral dust aerosols: A database for application or adiative transfer calculations, J. Aerosol Sci.,41, 501512.

Miller, R.L., & Tegen, I. (1998). Climate response to soil dust aerosols. J. Climate, 11, 3247-3267, doi:10.1175/1520-0442(1998)011<3247:CRTSDA>2.0.CO;2.

Muñoz, O., Volten, H., Hovenier, J.W., Nousiainen, T., Muinonen, K., Guirado, D., Moreno, F., & Waters, L.B.F.M., (2007). Scattering matrix of large Saharan dust particles: experiments and computations. Journal of Geophysical Research: Atmospheres, 112(D13).

Petzold, A., Rasp, K., Weinzierl, B., Esselborn, M., Hamburger, T., DöRNBRACK, A., Kandler, K., SchuüTZ, L., Knippertz, P., Fiebig, M., & Virkkula, A.K.I. (2009). Saharan dust absorption and refractive index from aircraft-based observations during SAMUM 2006. Tellus B: Chemical and Physical Meteorology, 61(1), pp.118-130.

Remer, L. A., and Coauthors, (2005). The MODIS aerosol algorithm, products, and validation. J. Atmos. Sci., 62, 947–973.

Remer, L. A., Kleidman, R. G., Levy, R. C., Kaufman, Y. J., Tanré, D., Mattoo, S., et al.. (2008). Global aerosol climatology from the MODIS satellite sensors. Journal Of Geophysical Research-Atmospheres, 113, D14S07. doi:10.1029/2007JD009661

Rosenfeld, D., Clavner,M., & Nirel,R. (2011), Pollution and dust aerosols modulating tropical cyclones intensities, Atmospheric Research,102, 66-76, doi.org/10.1016/j.atmosres.2011.06.006.

Sawyer, V.; Levy, R.C.; Mattoo, S.; Cureton, G.; Shi, Y.; Remer, L.A. Continuing the MODIS Dark Target Aerosol Time Series with VIIRS. *Remote Sens.* **2020**, *12*.

Sayer, A. M., Hsu, N. C., Lee, J., Kim, W. V., Dubovik, O., Dutcher, S. T. et al., (2018). Validation of SOAR VIIRS over-water aerosol retrievals and context within the global satellite aerosol data record. Journal of Geophysical Research: Atmospheres, 123, 13,496– 13,526. https://doi.org/10.1029/2018JD029465

Schutgens, N. A. J., Nakata, M., & Nakajima, T. (2013). Validation and empirical correction of MODIS AOT and AE over ocean, Atmos. Meas. Tech., 6, 2455–2475, https://doi.org/10.5194/amt-6-2455-2013.

Shao, Y., M. Klose, & Wyrwoll, K.-H. (2013), Recent global dust trend and connections to climate forcing, J. Geophys. Res. Atmos., 118, 11,107–11,118, doi:10.1002/jgrd.50836.

Shell, K. M., & Somerville, R. C. J. (2007). Sensitivity of climate forcing and response to dust optical properties in an idealized model. J. Geophys. Res., 112, D03206, doi:10.1029/2006JD007198.

Shi, Y., Levy, R.C, Eck, T. F., et al., (2019). Characterizing the 2015 Indonesia fire event using modified MODIS aerosol retrievals. Atmospheric Chemistry and Physics, 19 (1): 259-274 [10.5194/acp-19-259-2019]

Smirnov, A., et al. (2009), Maritime Aerosol Network as a component of Aerosol Robotic Network, J. Geophys. Res., 114, D06204, doi:10.1029/2008JD011257.

Sokolik, I. N., &Toon, O. B. (1999), Incorporation of mineralogical composition into models of the radiative properties of mineral aerosol from UV to IR wavelengths, J. Geophys. Res., 104(D8), 9423–9444, doi:10.1029/1998JD200048.

Song, Q., Z. Zhang, H. Yu, et al. (2018). Net radiative effects of dust in the tropical North Atlantic based on integrated satellite observations and in situ measurements. Atmospheric Chemistry and Physics, 18 (15): 11303-11322 [10.5194/acp-18-11303-2018]

Tang, X., Bi, L., Lin, W., Liu, D., Zhang, K., & Li, W. (2019). Backscattering ratios of soot-contaminated dusts at triple LiDAR wavelengths: T-matrix results. Opt. Express 27, A92-A116.

Tanré, D., Kaufman, Y. .J., Herman, M., & Mattoo, S. (1997). Remote sensing of aerosol properties over oceans using the MODIS/EOS spectral radiances. J. Geophys. Res., 102, (D14),. 16971–16988.

Torres, O., Ahn, C., & Chen, Z. (2013). Improvements to the OMI near-UV aerosol algorithm using A-train CALIOP and AIRS observations, Atmos. Meas. Tech., 6, 3257–3270, https://doi.org/10.5194/amt-6-3257-2013.

Wang, C., Platnick, S., Meyer, K., Zhang, Z., & Zhou, Y.(2020). A Machine Learning-Based Cloud Detection and Thermodynamic Phase Classification Algorithm using Passive Spectral Observations, Atmos. Meas. Tech. Discuss., https://doi.org/10.5194/amt-2019-409, in review.

Wiscombe, W. J. (1980). Improved Mie scattering algorithms, Appl. Optics, 19, 1505–1509, https://doi.org/10.1364/AO.19.001505.

Wyser, K. (1998). The effective radius in ice clouds. Journal of Climate. 11, 7, 1793-1802.

Yu, H., et al., (2006), A review of measurement based assessments of the aerosol direct radiative effect and forcing, Atmos. Chem. Phys., 6, 613–656.

Yu, H., Remer, L.A., Kahn, R. A., Chin, M., Zhang, Y. (2012). Satellite perspective of aerosol intercontinental transport: From qualitative tracking to quantitative characterization Atmospheric Research, 124 (2013), pp. 73-100, 10.1016/j.atmosres.2012.12.013

Yu, H., Chin, M., Bian, H., & et al. (2015). Quantification of Trans-Atlantic Dust Transport from Seven-year (2007-2013) Record of CALIPSO Lidar Measurements. Remote Sens. Environ, 159: 232-249 [10.1016/j.rse.2014.12.010]

Zhao, C., Liu, X., Leung, L. R., & S. Hagos, S. (2011). Radiative impact of mineral dust on monsoon precipitation variability over West Africa, Atmos. Chem. Phys., 11, 1879–1893, doi:10.5194/acp-11-1879-2011.

Table 1 Aerosol models (DT Model-1 and Model-8, Model-10)

	λ=0.47->0.87 μm	λ=1.24μm	λ=1.63μm	λ=2.11μm	r_g (μm)	σ (μm)	r_{eff} (μm)
Model-1	1.45-0.0035i	1.45-0.0035i	1.43-0.01i	1.40-0.005i	0.07	0.40	0.10
Model-8	1.53-0.003i (0.47) 1.53-0.001i (0.55) 1.53-0.000i (0.65) 1.53-0.00i (0.86)	1.46-0.000i	1.46-0.001i	1.46-0.000i	0.60	0.60	1.48
Model-10	Same as M8				0.5	0.6	1.23

Table 2. Time period and number of collocated dusty pixels from MODIS and AERONET/MAN sites. Note that this number reflects the number of individual MODIS retrievals within a 0.3 deg radius of the AERONET/MAN site and that there is no spatial averaging involved in the collocation.

	AERONET		MAN	
	Terra	Aqua	Terra	Aqua
Period	2000-2014	2002-2014	2004-2014	2004-2014
Dusty pixels	18775	19387	2955	3032

Table 3. Performance metrics of C6 and the new retrievals with a non-spherical dust model as compared with AERONET and MAN measurements for dusty pixels from the collocated datasets. EE is defined as ± (0.05 + 15%)

		Aqua-AERONET		Terra-AERONET		Aqua-MAN		Terra-MAN	
		C6	New	C6	New	C6	New	C6	New
AOD	bias	0.083	0.024	0.056	0.005	0.025	-0.008	0.055	0.013
	rms	0.228	0.168	0.191	0.145	0.098	0.073	0.221	0.127
	% within EE	64.35	82.30	69.76	85.61	86.18	95.09	70.66	88.53
	%Above EE	32.48	13.73	25.28	8.66	13.29	3.03	27.17	9.58
	% Below EE	3.17	3.97	4.95	5.73	0.53	1.88	2.17	1.90
AE	bias	0.134	0.060	0.211	0.013	0.229	-0.005	0.073	0.070
	rms	0.272	0.187	0.324	0.181	0.319	0.179	0.216	0.162

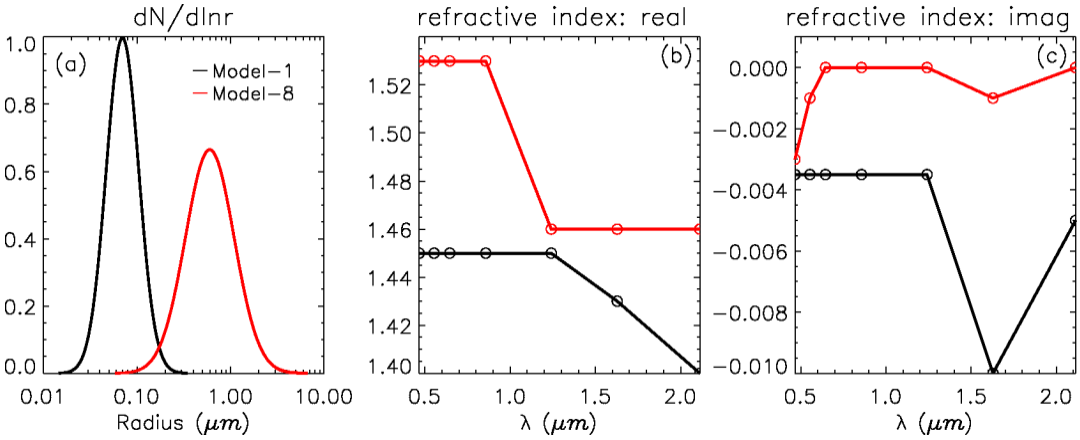

Figure 1. The number density distribution (a) and real (b) and imaginary (c) parts of the refractive index of DT aerosol Model-1 (black curves) and Model-8 (red curves).

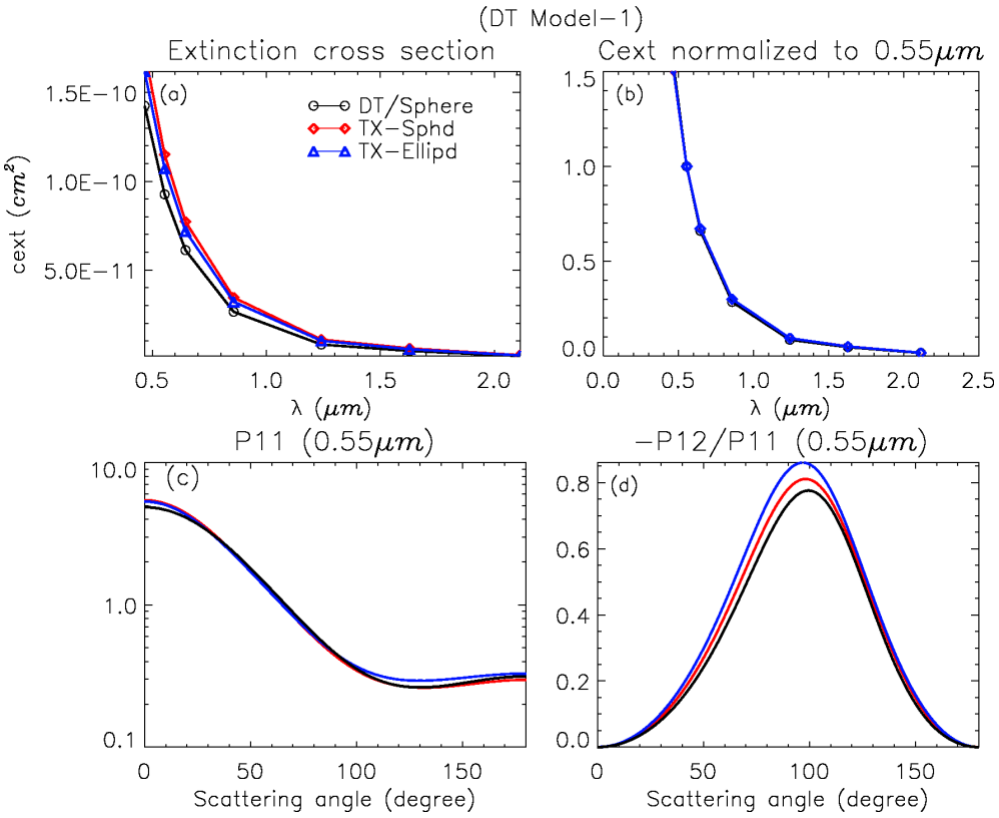

Figure 2. Sensitivity of optical properties to particle shapes for DT Model-1. Optical properties for spheres (DT/Sphere) are obtained from the DT Look Up Table, while a mixture of spheroids (TX-Sphd) and ellipsoids (TX-Ellipd) are obtained from the Texas A&M optical database. (a) Extinction cross section (Cext) and (b) extinction cross section normalized at 0.55 μm are shown for each wavelength used in the DT aerosol retrieval. (c) Phase function at 0.55 μm (P11) and (d) degree of linear polarization at 0.55 μm (-P12/P11) are shown as a function of scattering angle.

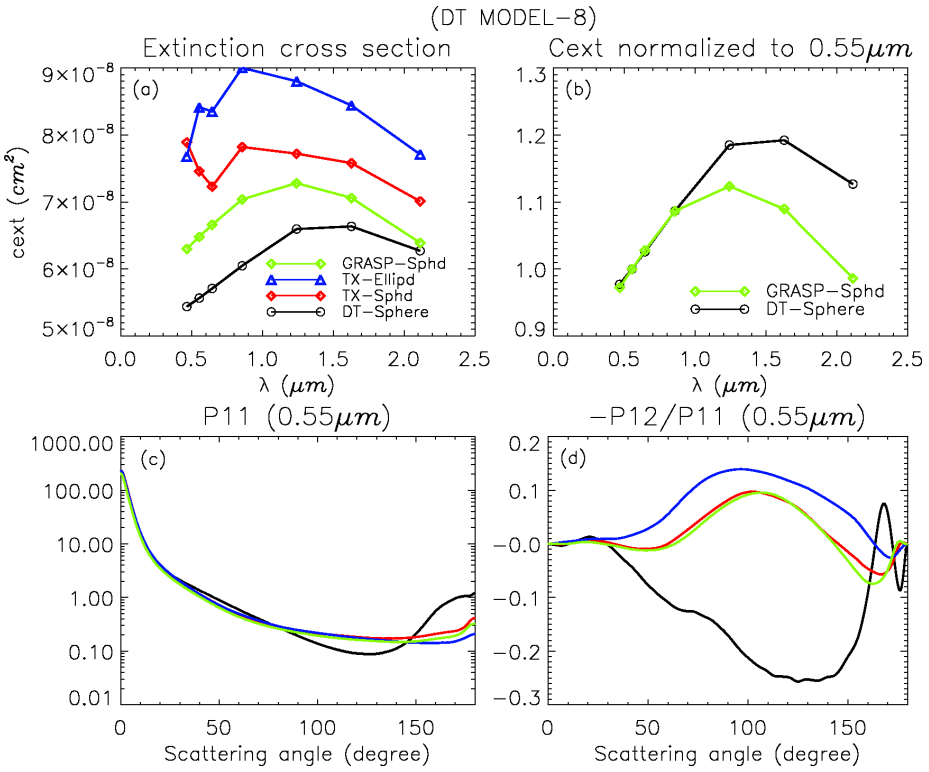

Figure 3. Sensitivity of optical properties to particle shapes for DT Model-8. Optical properties for spheres (DT-Sphere) are obtained from the DT Look Up Table, while, a mixture of spheroids (TX – Sphd) and ellipsoids (TX - Ellipd) are obtained from the Texas A&M optical database. The GRASP-Sphd uses the same mixture of spheroid particles as TX-Sphd but computes the optical properties with the GRASP GRASP's internal database instead of the Texas A&M database. (a) Extinction cross section (Cext) and (b) extinction cross section normalized to the value at 0.55 μm are shown for each wavelength used in the DT aerosol retrieval. (c) Phase function at 0.55 μm (P11) and (d) degree of linear polarization at 0.55 μm (-P12/P11) are shown as a function of scattering angle.

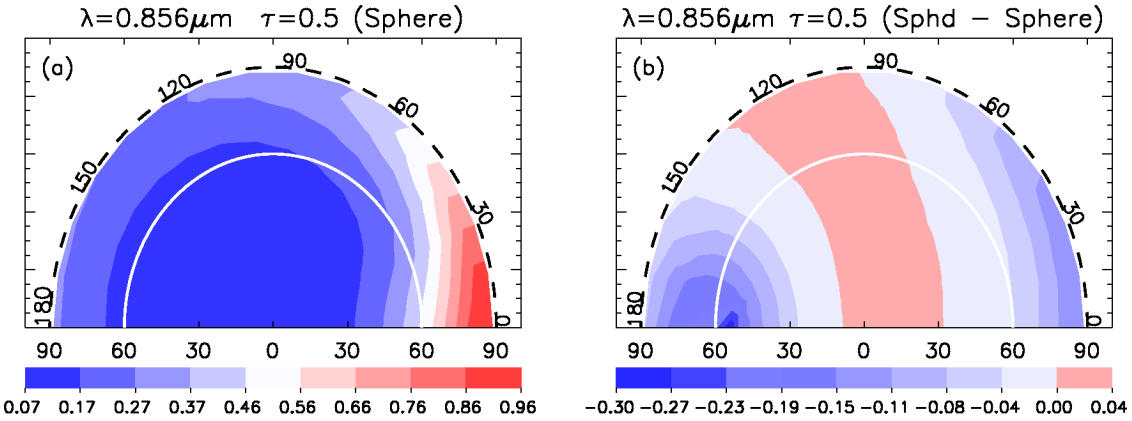

Figure 4. (a) LUT reflectance at 0.856 μm from MODEL-10 with spherical shape, (b) the reflectance difference when the particle shape in MODEL-10 is replaced with mixed spheroids. Reflectance is shown in polar coordinates. The values are plotted for LUT variables of τ=0.5, surface wind = 10m/s, and SZA = 54◦. View zenith angle ranges from 0-90° and relative azimuth angle ranges (counterclockwise) from 0-180°. The inner (white) arch encircles the view zenith angle approximates the range of MODIS observations.

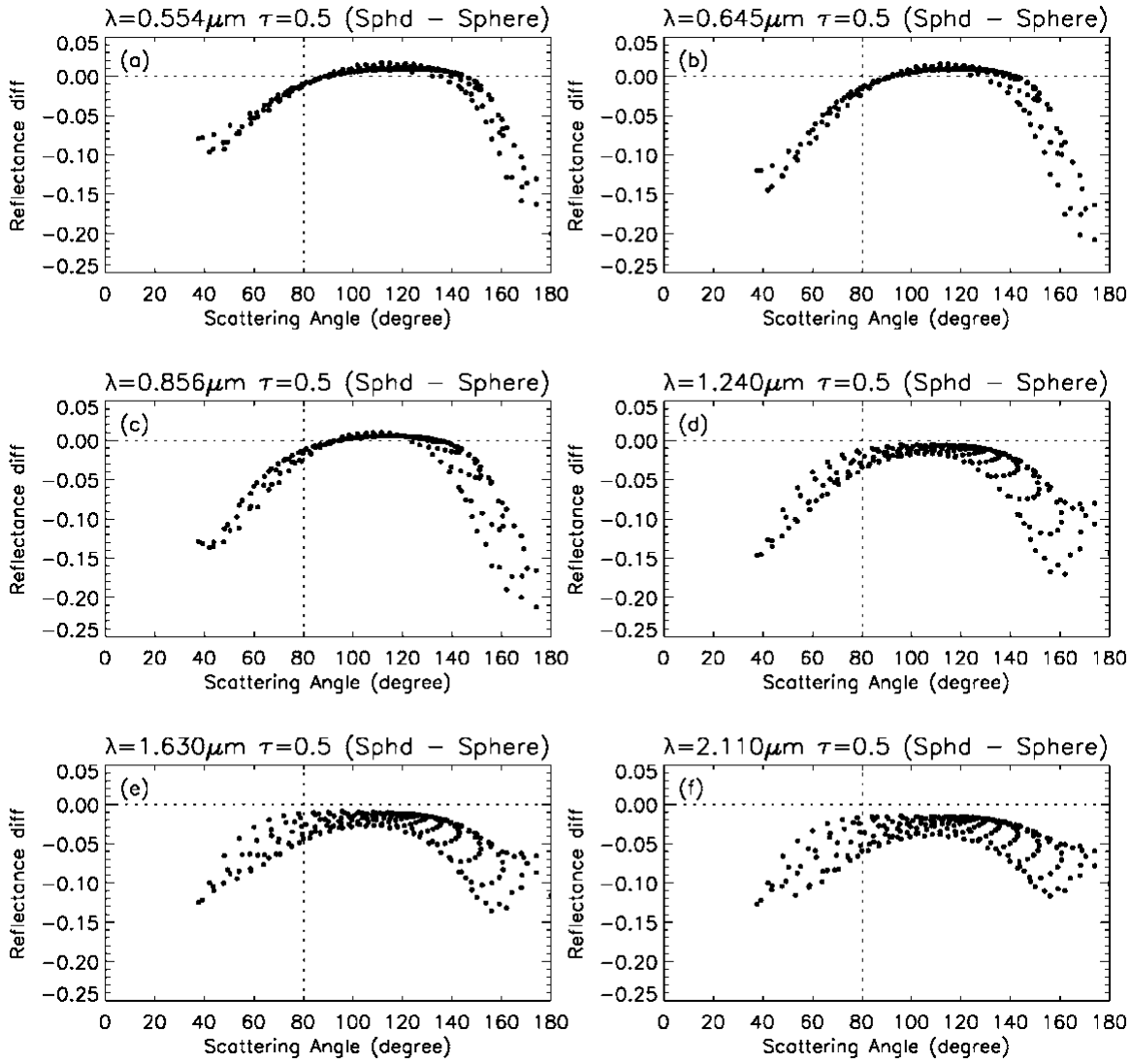

Figure 5. Reflectance difference in 6 DT aerosol retrieval wavelengths of Model-10 with spheroid and spherical particles as a function of scattering angle. Results shown are from with $\tau = 0.5$, surface wind = 10m/s and SZA = 54◦.

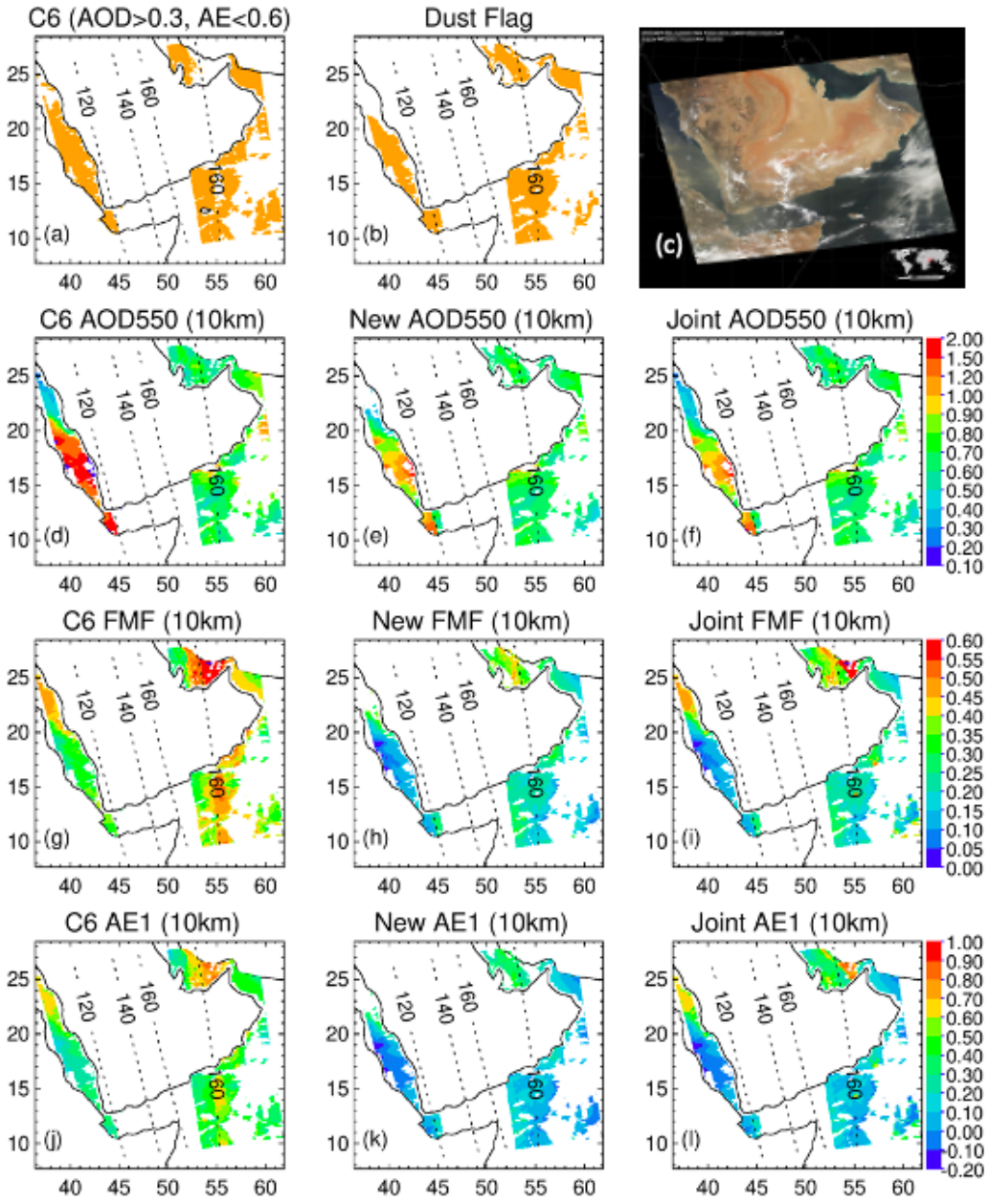

Figure 6. Sample retrievals for the MODIS-Aqua granule from 13 July, 2005 over the Arabian Peninsula. a) dust areas indicated by high AOD and low AE from the DT C6-retrieval, b): dust areas detected by the new dust detection algorithm. d, g, j): AOD, FMF and AE1 from DT C6 (spherical LUT) retrievals; e, h, k): retrievals using new dust model (for detected dust pixels only); f, i, l): Joint products. Included in each panel are contours of scattering angle (Θ).

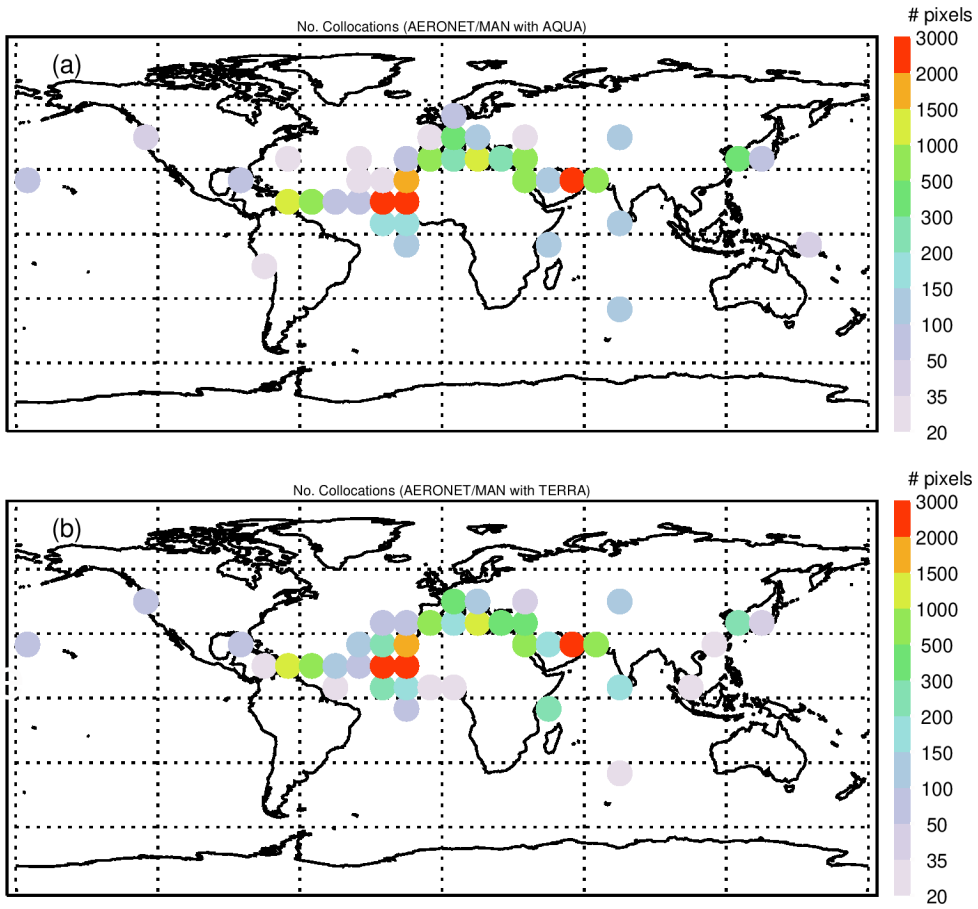

Figure 7. (a) Number of AERONET and MAN dusty pixels collocated with AQUA MODIS in 10° latitude x10° longitude boxes. (b) The same as (a) but for collocation with TERRA MODIS.

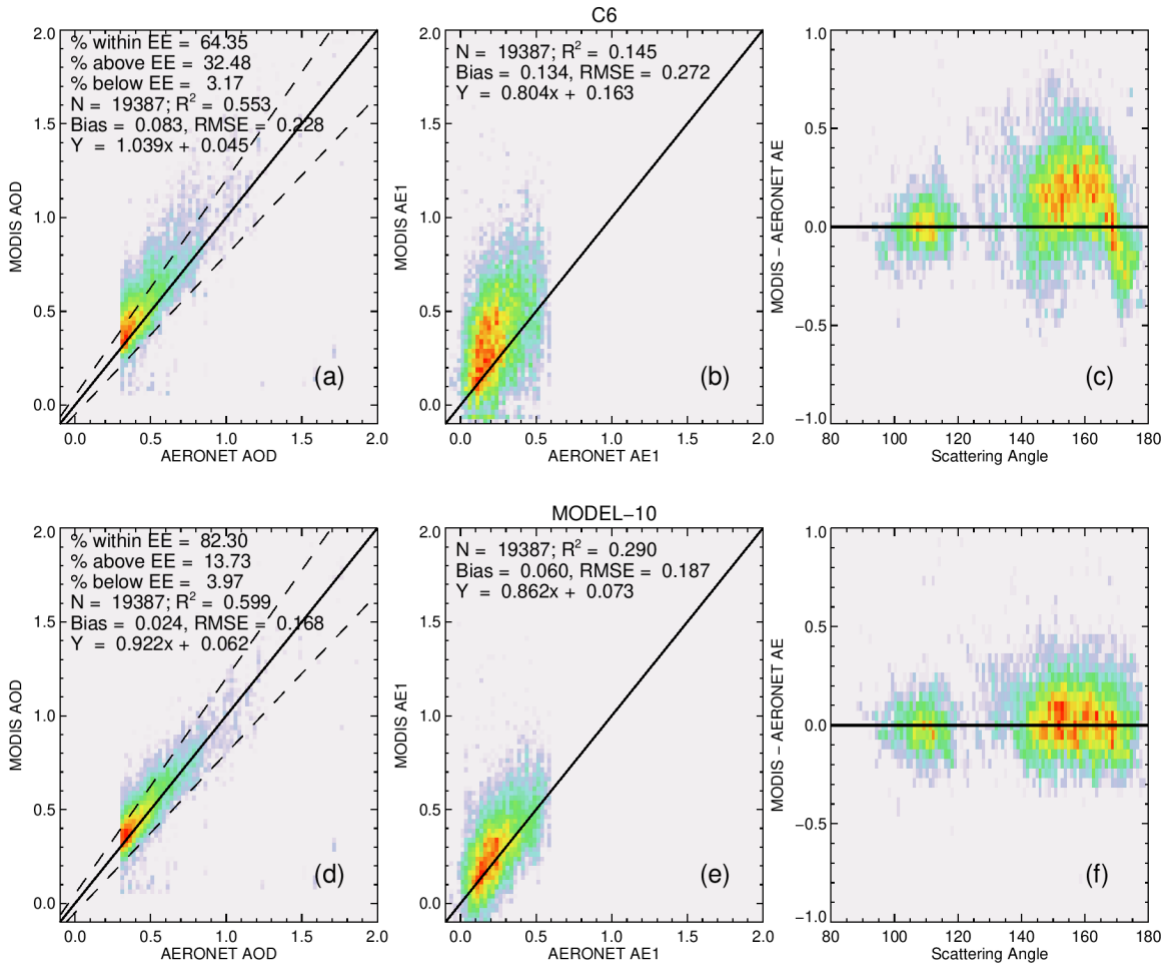

Figure 8. Comparison of dust retrievals from DT Version C6 and the new dust model (Model-10) for collocations between AERONET and Aqua dusty pixels. a) scatter plot of AOD at 0.55 μm between C6 and AERONET; b) scatter plot of AE1 between C6 and AERONET; c) MODIS – AERONET AE1 bias as a function of scattering angle. Bottom panel is the same as the top panel except for the new retrieval with Model-10.

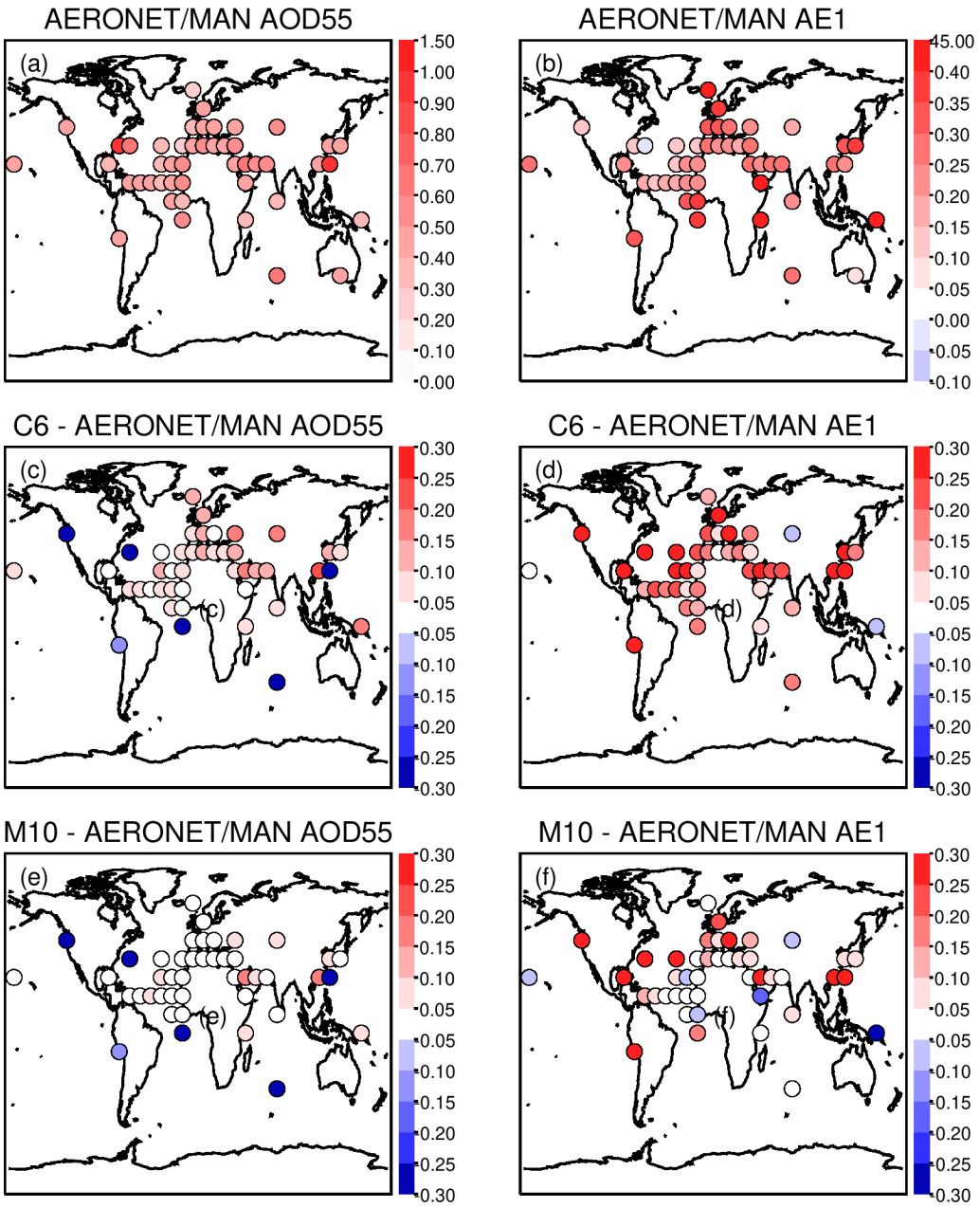

Figure 9. (a) Long term mean AOD at 0.55 μm and (b) AE1 for 10o latitude x 10o longitude boxes from AERONET/MAN measurements using the collocated data set with Aqua. Mean bias of C6 DT retrievals as compared to AERONET/MAN in each 10o latitude x 10o longitude box for (c) AOD at 0.55 μm and (d) AE1. Mean bias of retrievals using the non-spherical dust model (Model-10) as compared to AERONET/MAN in each 10o latitude x 10o longitude box for (e) AOD at 0.55 μm and (f) AE1.

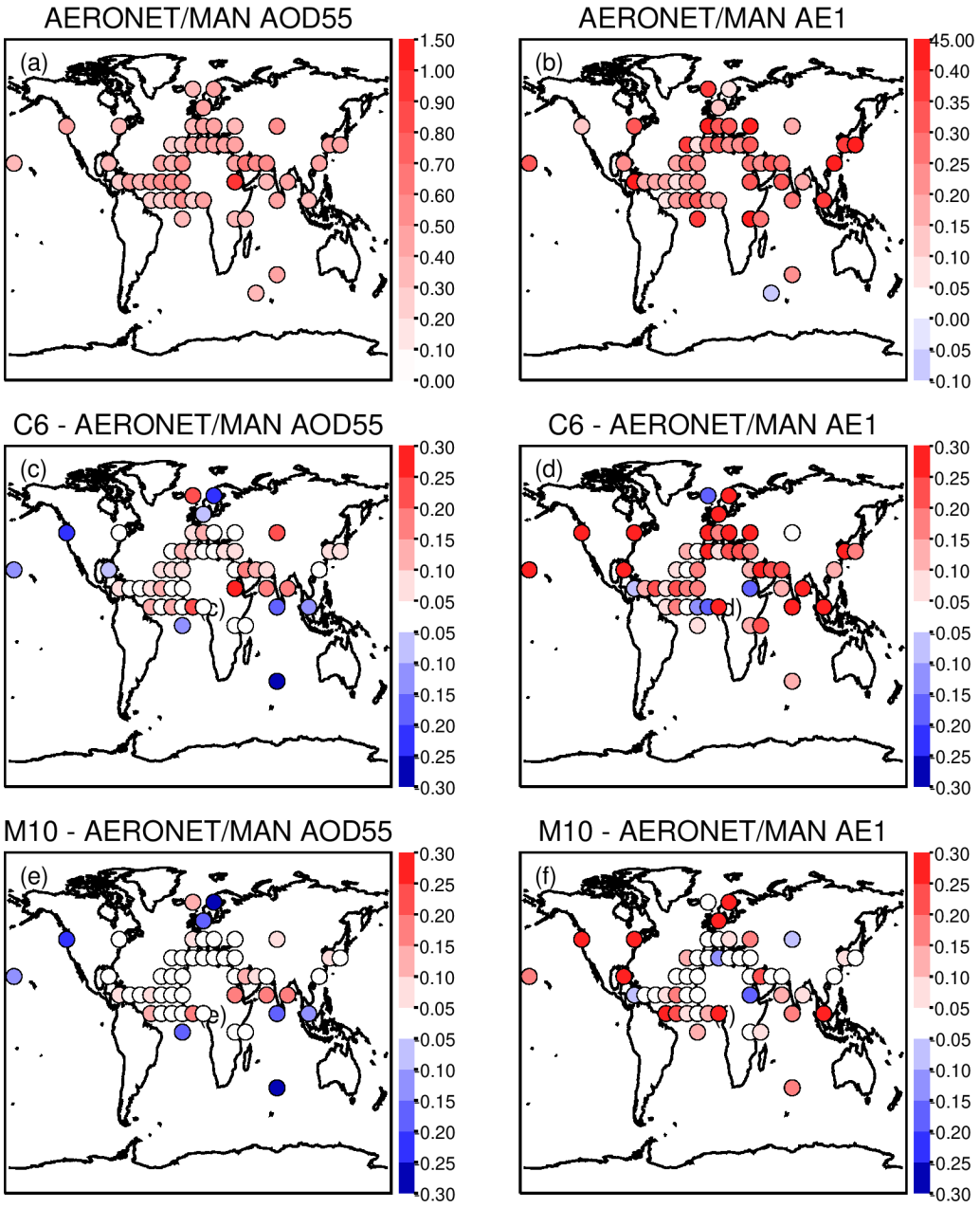

Figure 10. Same as Figure 9 but for the collocated Terra and AERONET/MAN data set.

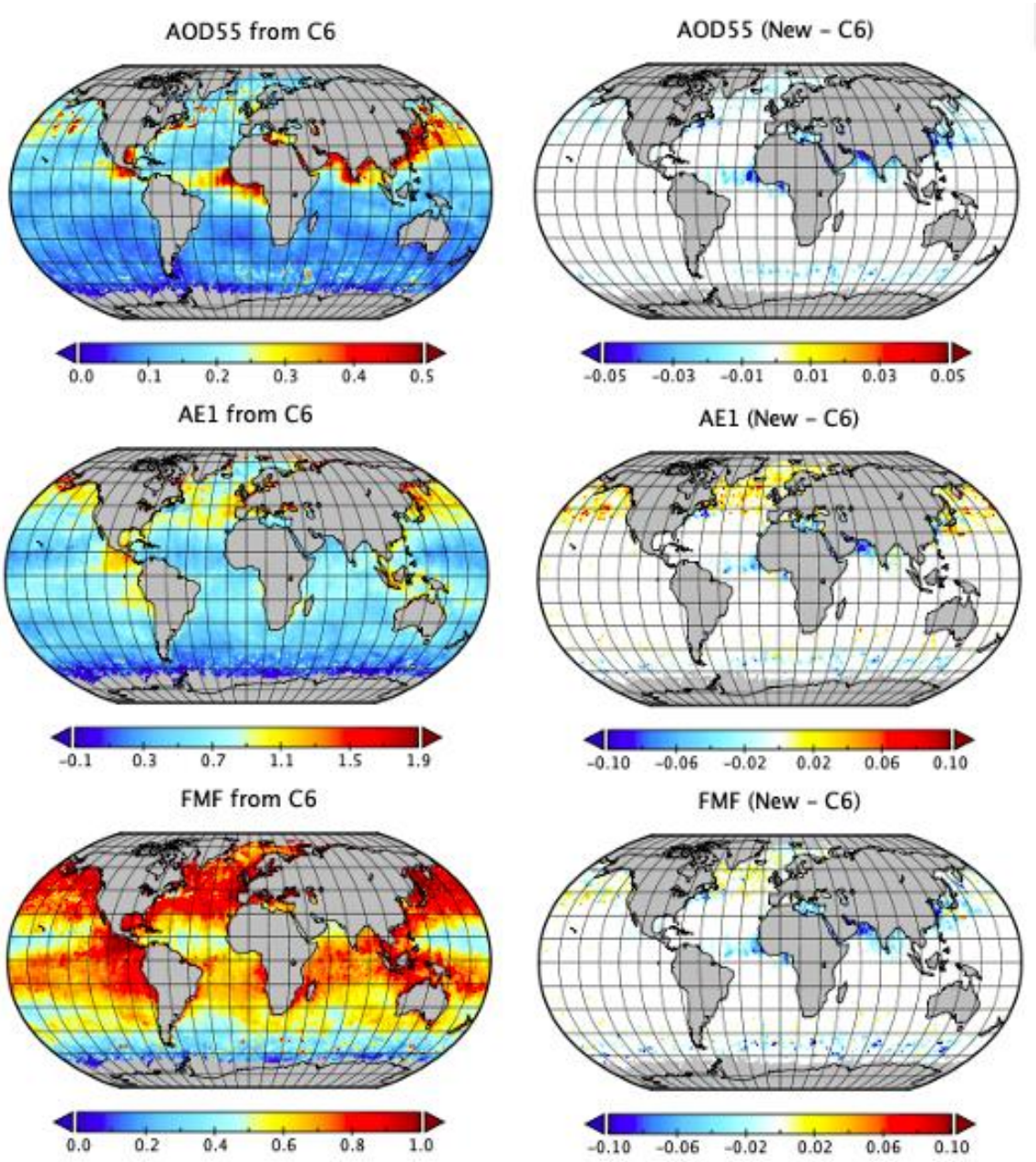

Figure 11. Mean AOD, AE1 and FMF from the C6 DT algorithm during April 12-May 11, 2011 (left column) and the mean difference between C6 and retrievals with new dust model for detected dusty pixels (New – C6).

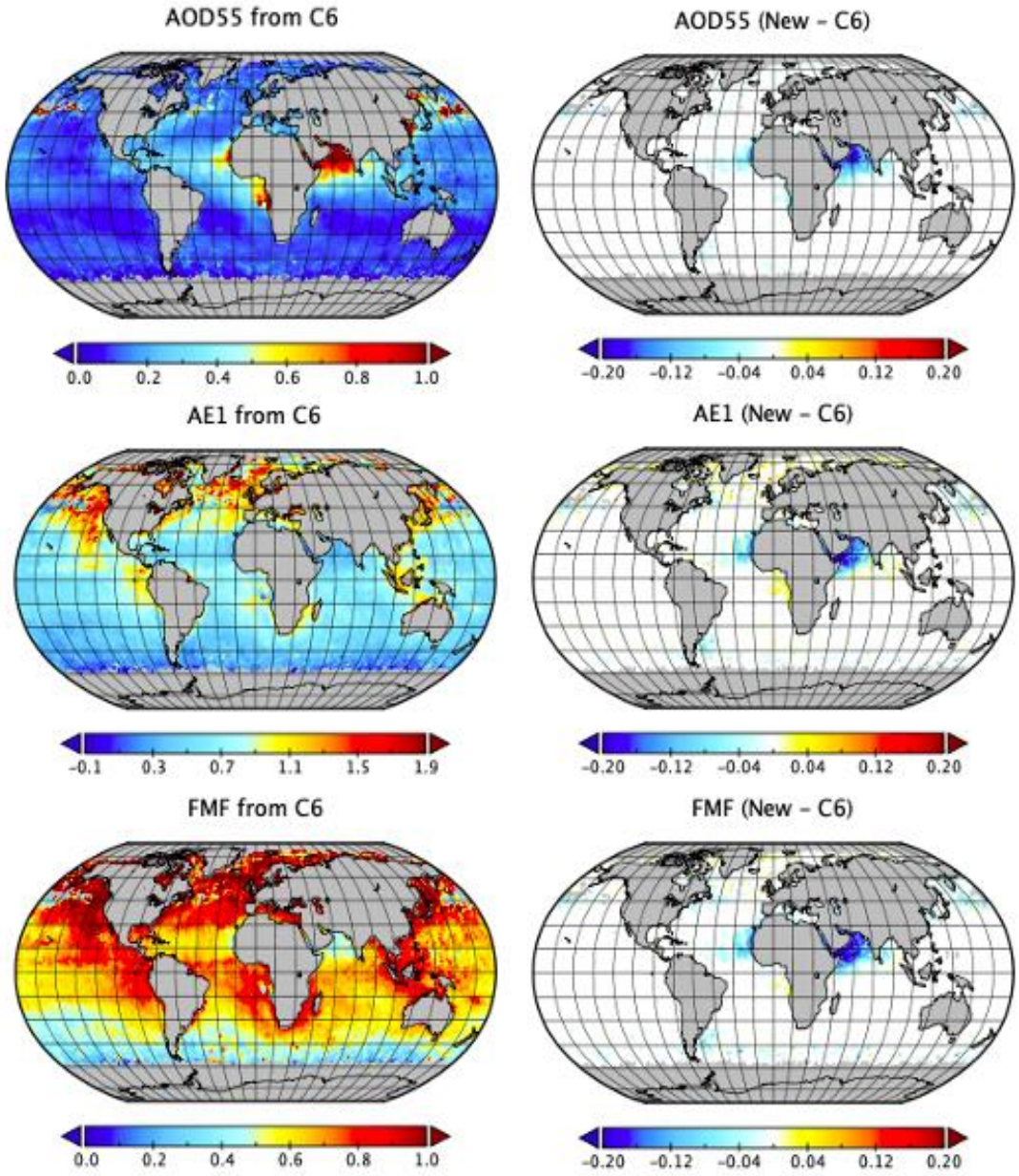

Figure 12. Same as Figure 11 but for July 2011.